

# Large-scale simulation of ground motion amplification considering 3D topography and subsurface soils



Gang Wang & Chunyang Du

*Department of Civil and Environmental Engineering, The Hong Kong University of Science and Technology*

Duruo Huang

*Department of Civil and Environmental Engineering and Institute for Advanced Study, The Hong Kong University of Science and Technology*

## ABSTRACT

Amplification of seismic waves due to surface topography and subsurface soils has often been observed to cause intensive damage in past earthquakes. However, due to its complexity, topographic amplification has not yet been considered in most seismic design codes. In this study, we simulate ground-motion amplification based on 3D Spectral Element Method, using Hong Kong island as a local testbed site. The analyses revealed that topography amplification of ground motions is frequency dependent. By assuming the site is made of homogenous rock, the amplification factor can be parameterized using a scale-dependent topographic feature -- the smoothed curvature. Amplification of high frequency wave is correlated with curvature smoothed over a small length scale. On the other hand, amplification of long-period waves is correlated with large-scale topography features. The maximum topography amplification generally ranges from 1.6 to 2.0 in the protruded areas. Moreover, the influence of subsurface soils on the ground-motion amplification is studied. It is found that the ground-motion amplification pattern is significantly influenced by the thickness of the soil layer. Compared with the homogeneous rock case, the amplification pattern becomes closely correlated to smaller-scale topographic features as well as slope angles. Finally, a unified prediction model is proposed to account for different soil depths and input wave frequencies. Our study shows that the prediction model can give accurate results with a standard deviation of residuals less than 0.15.

## 1 INTRODUCTION

Surface topography and subsurface soil structure can significantly amplify ground motions during earthquakes. (Spudich et al. 1996; Trifunac et al. 1971). However, due to its complexity, topography amplification has not yet been well understood. It is also barely considered in most seismic design codes, with a few exceptions such as the Eurocode 8 (CEN 1998). Using a simplified classification of ridge geometry and slope angle, EU8 prescribes a topographic amplification factor which is frequency-independent. On the other hand, significantly larger topography amplification in order of 10 to 20 has been observed through instrumented data. As is against EU8, the topography amplification is also found to be frequency-dependent (Burjanek et al. 2014). Meanwhile, amplification of ground motions in realistic sites is due to the coupled 3D topography and subsurface soil effects. It is crucial to identify the key factor that influence the coupling effects of 3D soil-topography amplification, and develop a simplified parametric model for practical applications.

Numerous numerical studies have conducted to reveal the topographic amplification phenomenon (e.g. Ashford et al. 1997; Assimaki et al. 2005). However, in these analyses, simple 2D topography geometries are often used and the soil is assumed to be a uniform viscoelastic material. The numerical simulations usually result in an amplification factor less than 2, which tends to underestimate the field data.

Hong Kong is used as the test bed in this study. In this place, many buildings and infrastructures were built on hill tops and steep slopes due to paucity of land. Owing to the subtropical climate, the volcanic and granitic rocks are subjected to extensive weathering, varying from Grade I (fresh rock) to Grade VI (residual soils) (Arup, 2012). Therefore, investigating the extent of soil cover and weathered rock profiles in the study region is also very important. The latest Chinese Seismic Code (China Code 2010) prescribes a peak ground acceleration of 0.12 g for the 475-year return period on "rock" outcrop. It is noted that the obtained design ground-motion are only applicable for a level ground. To date, scientifically based standard for seismic design of buildings on steep slopes is still not available.

## 2 METHODOLOGY AND MODEL SETUP

3D Spectral Element Method (SEM) is used for the simulation of wave propagation in this study. The SEM is a high-order finite element method and the main advantage of SEM is that it combines the flexibility of finite element method and the accuracy of pseudospectral techniques (Komatiitsch et al. 2004). It can also be easily implemented in parallel computing because the mass matrix is exactly diagonal when using Lagrange polynomials and Gauss-Lobatto-Legendre quadrature. In this paper we modify and use the open source software package SPECSEM3D Cartesian first developed by Komatiitsch and Vilotte (1998) in France and then by

Komatitsch and Tromp (1999) in the United States to conduct all the simulations.

Figure 1 illustrated an elevation map of western part of Hong Kong Island. The dimension of the computational domain is  $8 \text{ km} \times 9 \text{ km}$ . The highest point in this region, Victoria Peak, is about 554 m above the sea level. The illustration of constructed SEM model is shown in Figure 2. A Digital Elevation Model (DEM) of  $0.5 \text{ m} \times 0.5 \text{ m}$  resolution is provided by the Geotechnical Engineering Office of the Civil Engineering and Development Department of Hong Kong SAR, which is used to extract elevation data to construct 3D numerical model and calculate topographic curvatures. The elevation data extracted from the DEM is fine enough to cover very detailed topographic features of the study area.

Uniform ground excitation is input at the base of the model. Lysmer-Kuhlemeyer transmitting boundary is implemented to mimic the infinite half space at the bottom, and absorbing boundaries are used on the sides to avoid wave reflection from the boundary.

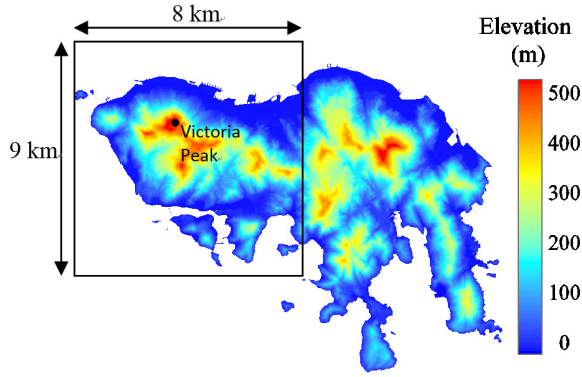


Figure 1: Hong Kong Island elevation map

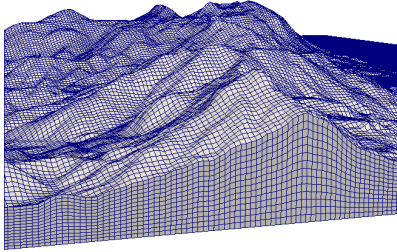


Figure 2: Illustration of 3D SEM mesh

### 3 HOMOGENEOUS ROCK CASE

Recently, Wang et al. (2016) studied the topographic amplification of ground motions for Hong Kong Island, by assuming the site is made of uniform and linearly elastic rock with  $V_s=1000 \text{ m/s}$ . Surface soil cover is not considered at that stage. Ricker wavelet is used as acceleration input in the simulations, with predominate frequency of the wavelet varying from 0.5 Hz to 5 Hz. The amplification factor is defined as the PGA recorded on the slope surface divided by the PGA recorded on the level ground.

### 3.1 Simulation Results

Figure 3 (a) (b) show amplification factor maps under 5 Hz and 1 Hz wavelet excitation, where the maximum amplification factor is 2.1 and 1.9, respectively. It is obvious that the amplification/de-amplification is closely related to very localized topographic features under the high frequency (5 Hz) excitation. The results are in line with the generally accepted notion that long wavelengths mainly influence large features while short ones influence small features.

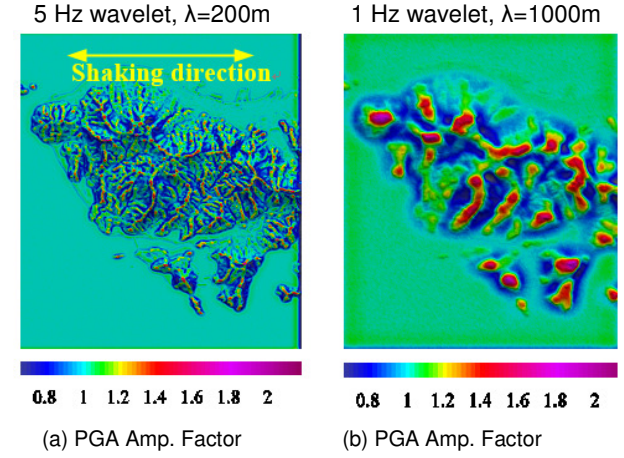


Figure 3: PGA amplification factor maps excited by different frequency wavelet

### 3.2 Smoothed Topographic Curvature

We use the method developed by Zevenbergen and Thorne (1987) and Moore (1991) to quantify the topographic curvature. In this method, general curvature is defined as the summation of second derivative of elevation in two horizontal directions. If the Digital Elevation Model (DEM) of the region  $\mathbf{E}$  is evenly spaced elevation values with space increment  $h$ , the DEM curvature  $\mathbf{C}$  could be calculated as

$$\mathbf{C}(x_i, y_i) = \mathbf{E}''(x_i, y_i) \approx -2(\delta + \eta) \times 100 \quad [1]$$

where  $\delta$  and  $\eta$  are second derivative of elevation in  $x$  and  $y$  directions as

$$\delta = \frac{1}{h^2} \left[ \frac{\mathbf{E}(x_{i-1}, y_i) + \mathbf{E}(x_{i+1}, y_i)}{2} - \mathbf{E}(x_i, y_i) \right], \text{ and}$$

$$\eta = \frac{1}{h^2} \left[ \frac{\mathbf{E}(x_i, y_{i-1}) + \mathbf{E}(x_i, y_{i+1})}{2} - \mathbf{E}(x_i, y_i) \right] \quad [2]$$

Maufroy et al. (2015) introduced a smoothed curvature to account for the influence of the length scale. A box blur smoothing operator is used here, which consists in a double convolution of matrix  $\mathbf{C}$  with an  $n \times n$  unit matrix:

$$\mathbf{C}_s = \frac{1}{n^4} \left[ \mathbf{C} * \begin{pmatrix} 1 & \dots & 1 \\ \vdots & \ddots & \vdots \\ 1 & \dots & 1 \end{pmatrix}_{n \times n} * \begin{pmatrix} 1 & \dots & 1 \\ \vdots & \ddots & \vdots \\ 1 & \dots & 1 \end{pmatrix}_{n \times n} \right] \quad [3]$$

where  $n$  is the space number and  $h$  is the space increment.

According to Maufroy et al. (2015), the smoothing length is defined as  $L_s = 2 \times n \times h$ . The general curvature maps smoothed over different smoothing lengths are shown in Figure 4. Apparently, more localized topography (convex/concave) details can be captured if a shorter smoothing length is used.

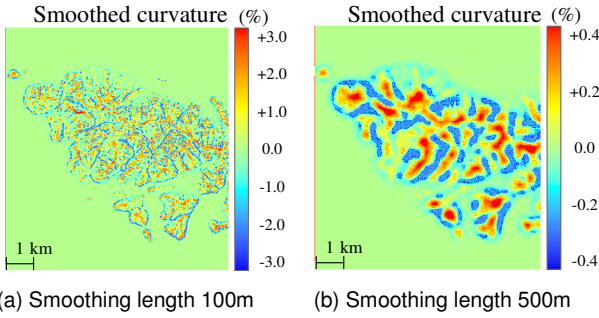


Figure 4: Smoothed curvatures using different smoothing lengths

### 3.3 Relationship between Smoothed Curvature and Topographic Amplification Factors

Regression analysis is performed to determine the relationship between smoothing lengths and amplification factors. For each smoothing length, the coefficient of determination  $R^2$  is calculated and plotted in Figure 5. It is found that the amplification factor (AF) can be best correlated (with a largest  $R^2$ ) with the smoothed curvature ( $C_s$ ), if the smoothing length  $L_s$  is half of the input wavelength, i.e.,  $L_s = \lambda_{Rock}/2$ , which is referred as the 'characteristic smoothing length'.

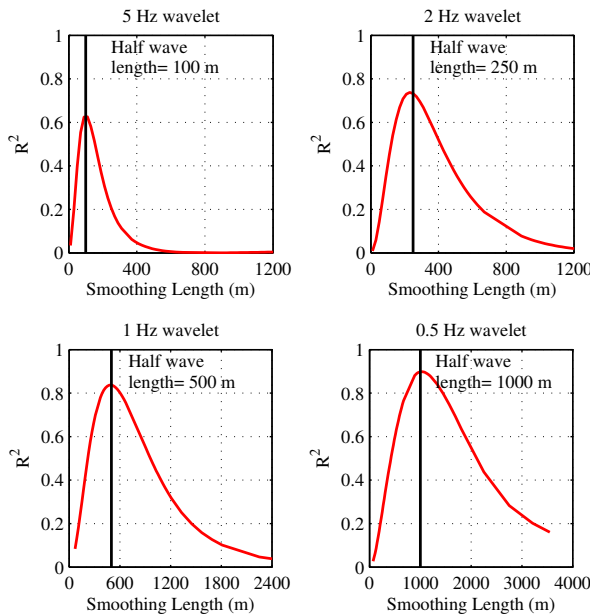


Figure 5: Coefficient of determination  $R^2$  between different smoothing lengths and amplification factors

Figure 6 shows the topographic amplification factor versus the smoothed curvature. The data can be cast into an exponential form:

$$AF_{\text{Homo}}^{3D}(\lambda_{\text{Rock}}, C_s) = \exp[a(\lambda_{\text{Rock}}) \times C_s(L_s)] \quad [4]$$

where  $a(\lambda_{\text{Rock}}) = 9.90 \times 10^{-4} \lambda_{\text{Rock}} - 0.083$  and  $\lambda_{\text{Rock}}$  is the wavelength in rock (unit in meter,  $\lambda_{\text{Rock}} = V_{s, \text{Rock}}/f$ ).  $C_s$  is the curvature smoothed over the characteristic length  $L_s = \lambda_{\text{Rock}}/2$ . Equation 4 manifests that the frequency-dependent amplification is related to a scale-dependent topographic feature, similar to Maufroy et al. (2015). In addition, when the frequency of input wavelet becomes smaller,  $R^2$  becomes larger and the slope of the fitted exponential curves becomes steeper. All the curves approximately pass through the point of (0,1), which is reasonable because for the special case when the surface is flat, there is no amplification or deamplification.

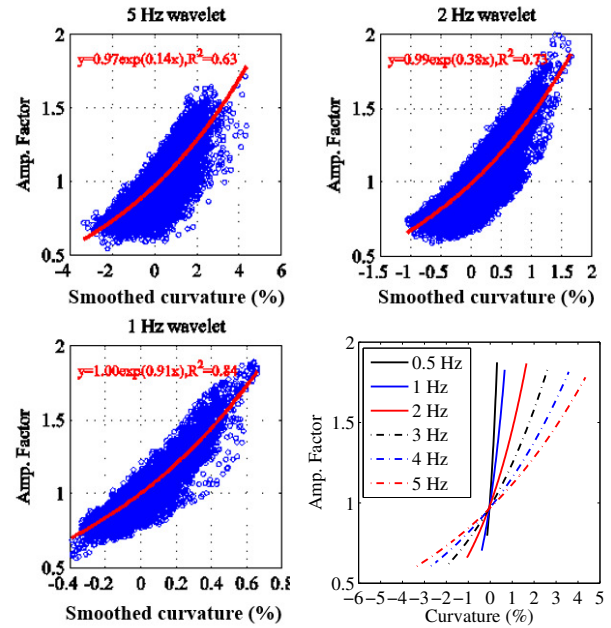


Figure 6: Correlation between amplification factor and curvature smoothed over characteristic length ( $L_s = \lambda_{\text{rock}}/2$ )

## 4 INFLUENCE OF SUBSURFACE SOILS ON GROUND MOTION AMPLIFICATION

In reality, a layer of soils is often present at the topographic surface during to extensive weathering of in-situ rock. The influence of surface soils on ground-motion amplification is considered in the following study. At the present stage, soil nonlinearity is not considered. So, the soil is assumed to be linearly elastic with shear wave velocity 200 m/s, which is typical value for weathered surface soils in Hong Kong (Arup 2012). Thus, the wavelength in soil layer is 1/5 of that in rock, that is  $\lambda_{\text{Soil}} = 1/5 \lambda_{\text{Rock}}$ . Three-dimensional SEM simulations are conducted considering a layer of soil with a uniform depth. The predominate frequencies of the input wavelet are 1 Hz, 2 Hz and 5 Hz, respectively. Accordingly, the

corresponding wavelength in soil,  $\lambda_{\text{Soil}}$ , equals to 200 m, 100 m and 40 m.

#### 4.1 Amplification Factor of Layered Soils

In the following studies, the amplification factor is defined as the PGA recorded on the soil surface divided by the PGA recorded on the level ground for the soil, that is  $AF = AF_{\text{Layered}}^{3D} / AF_{\text{Soil}}^{1D}$ , where  $AF_{\text{Soil}}^{1D}$  can be obtained from 1D site response analyses. Figure 7 (a) shows the  $AF_{\text{Soil}}^{1D}$  obtained from 1D response analyses is a function of soil depths and frequencies of wavelet excitation. If the soil depth is normalized by the wavelength  $\lambda_{\text{Soil}}$ , the amplification factors coincide for different input frequencies, as shown in Figure 7 (b). This indicates that the 1D soil amplification factor,  $AF_{\text{Soil}}^{1D}$ , is only dependent on the soil depths normalized by the soil wavelength. The  $AF_{\text{Soil}}^{1D}$  reaches a peak value of 2.35 when the soil depth equals to  $0.2\lambda_{\text{Soil}}$ .

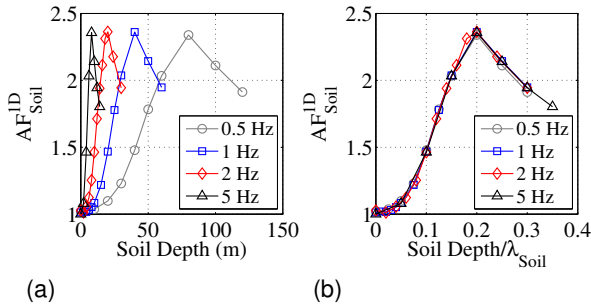


Figure 7:  $AF_{\text{Soil}}^{1D}$  obtained from 1D response analysis

The amplification factor ( $AF_{\text{Layered}}^{3D} / AF_{\text{Soil}}^{1D}$ ) of 1 Hz excitation case is shown in Figure 8. The four figures are homogeneous rock case (soil depth=0 m) and cases with soil depth of 20 m, 40 m and 60 m respectively.

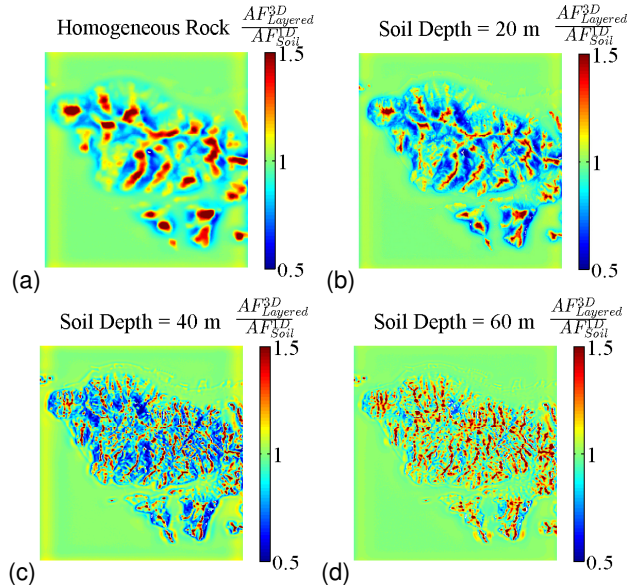


Figure 8: PGA amplification factor  $AF = AF_{\text{Layered}}^{3D} / AF_{\text{Soil}}^{1D}$  maps excited by 1 Hz wavelet with different soil depths

Due to the existence of surface soils, the amplification pattern has changed significantly compared with the homogeneous rock case, which is closely correlated to large-scale topographic features. With an increasing soil depth, the amplification zones become narrower, although they are still around the mountain ridges, as shown in Figure 8 (a) and (b). If the soil depth further increases, the amplification pattern generally change to the case of a homogeneous soil site, with the amplification pattern more closely correlated to small-scale topographic features, i.e., curvatures smoothed using a smaller smoothing length. This is reasonable because the wavelength in the surface soils is 1/5 of that in rock,  $\lambda_{\text{Soil}} = 1/5 \lambda_{\text{Rock}}$ , therefore, the presence of the soil layer tends to be influence by small-scale topographic features. It is also interesting to notice that when the soil depth is larger than a certain limit, the amplification pattern will no longer change significantly and can be approximated as a homogeneous soil case.

#### 4.2 Influence of Subsurface Soil Depth on Characteristic Smoothing Length

In order to obtain the characteristic smoothing length for the layered case, parametric study is conducted using 1Hz, 2Hz and 5Hz wavelet excitation by assuming different soil depths. The results are compared with the homogeneous rock case ( $SD=0m$ ) in Figure 9, where the characteristic smoothing length for homogenous rock case ( $L_s = \lambda_{\text{Rock}}/2$ ) is highlighted using a solid line for each case.

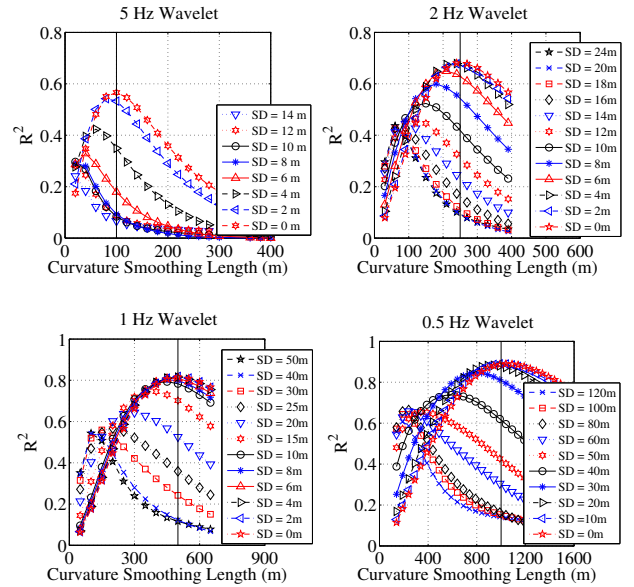


Figure 9:  $R^2$  obtained between different smoothing lengths and amplification factors.

It is observed that the characteristic smoothing length (corresponding to the maximum  $R^2$ ) becomes smaller with an increasing soil depth. This is due to the fact that  $\lambda_{\text{Soil}}$  is much shorter than  $\lambda_{\text{Rock}}$ , therefore, the size of influenced features should be smaller. Moreover, the maximum  $R^2$  also decreases with an increasing soil depth. When the

soil reaches a certain depth, no significant change is observed for the characteristic smoothing length and its associated  $R^2$ . These results are consistent with conclusions derived previously from the amplification maps.

Finally, the relation between the modified characteristic smoothing length ( $L_s$ ) and soil depth (SD) is shown in Figure 10(a). If  $L_s$  and SD are normalized by  $\lambda_{\text{Soil}}$ , Figure 10(a) can turn into a rather unified relationship, shown as the dashed red line in Figure 10(b). For the layered site,  $L_s$  decreases linearly from  $2.5\lambda_{\text{Soil}}$  (corresponding to a homogenous rock case,  $0.5\lambda_{\text{Rock}}$ ) to  $0.5\lambda_{\text{Soil}}$ , when the soil depth increases from 0 to  $0.2\lambda_{\text{Soil}}$ . The data also indicates that when the soil depth becomes greater than  $0.2\lambda_{\text{Soil}}$ ,  $L_s$  remains as  $0.5\lambda_{\text{Soil}}$  without influence of the soil depth, which corresponds to a homogenous soil case. It is important to note that  $0.2\lambda_{\text{Soil}}$  correspond somewhat to the the natural frequency of the soil column, which would occur at  $SD=0.25\lambda_{\text{Soil}}$  for the first mode. This implies the relationship between the soil depth and the shear-wave velocity of the subsurface soils is very important in quantifying the effect of topographic amplification.

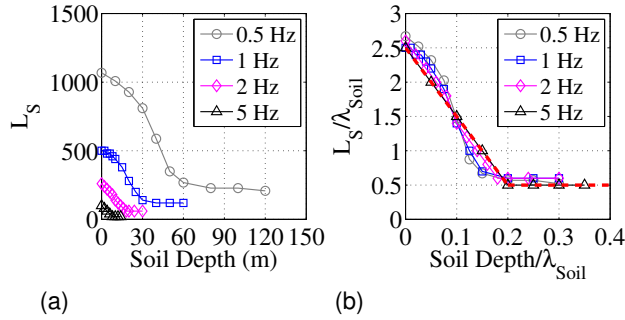


Figure 10: Modified characteristic length for different frequency wavelets with different soil depths

#### 4.3 Prediction Equations for Topographic Amplification

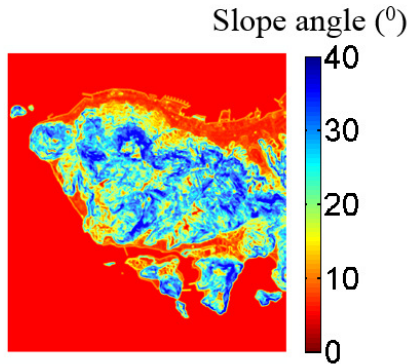


Figure 11: Slope angle map

Although it is tempting to use a simple functional form of  $C_s$ , such as Equation 4, to correlate the amplification factor,  $AF = AF_{\text{Layered}}^{3D} / AF_{\text{Soil}}^{1D}$ , for the layer case, it is found that the AF is also dependent on the slope angles by

regression analyses, especially, when the slope angle is greater than  $15^\circ$ . The AF prediction can be significantly improved by introducing a linear term with respect to slope angles. Therefore, the following functional form is proposed:

$$\ln\left(\frac{AF_{\text{Layered}}^{3D}}{AF_{\text{Soil}}^{1D}}\right) = \begin{cases} a(L_s, SD) \times C_s(L_s) + \epsilon, & \text{for } \theta < \theta_0 \\ a(L_s, SD) \times C_s(L_s) + b(SD) \times (\theta - \theta_0) + \epsilon, & \text{for } \theta \geq \theta_0 \end{cases} \quad [5]$$

where SD is the soil depth (in m),  $a(L_s, SD)$  and  $b(SD)$  are parameters to be determined,  $C_s(L_s)$  is the curvature smoothed over the characteristic length shown in Figure 10 (b),  $\theta$  is the slope angle (in degree) as shown in Figure 11, and  $\theta_0 = 15^\circ$  according to the regression analyses.  $\epsilon$  is the residuals that follow a normal distribution with a zero mean and a standard deviation of  $\sigma = \text{std}(\epsilon)$ .

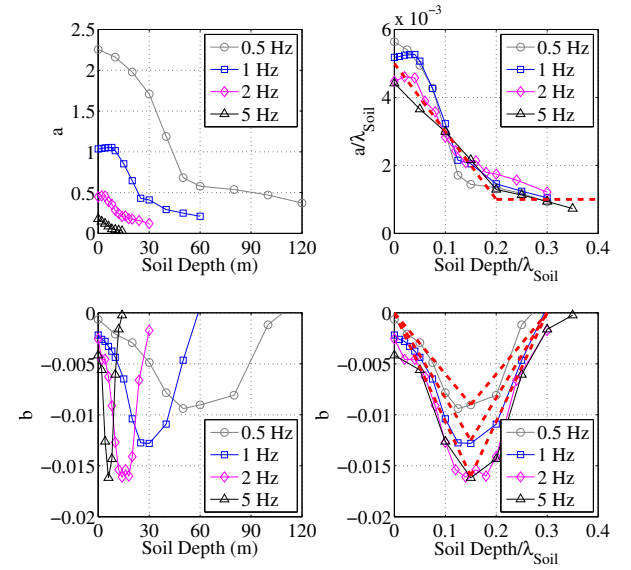


Figure 12: Parameter  $a(L_s, SD)$  and  $b(SD)$  derived for different soil depths and frequencies

The parameters  $a(L_s, SD)$  and  $b(SD)$  values for different wavelet frequencies and soil depths are obtained by regression analysis and are illustrated in Figure 12. If these two parameters are normalized by the wavelength in the soil,  $\lambda_{\text{Soil}}$ , a unified relation can be obtained for these two parameters, as represented by the red dash lines in Figure 12. The parameter  $a(L_s, SD)$  for the curvature decreases when the soil depth is less than  $0.2\lambda_{\text{Soil}}$  and remains to be constant for deeper soils. The parameter  $b(SD)$  for the slope angle first decreases and then increases to zero. Interestingly, a minimum value of  $b$  (termed as  $b_0$ ) occurs when the soil depth is  $0.15\lambda_{\text{Soil}}$  for all wave frequencies. This trend also indicates that when the soils are deeper than  $0.3\lambda_{\text{Soil}}$ , the influence of slope angle on the topographic amplification becomes negligible, the  $b$  value becomes zero.

Figure 12 further illustrates dependency of  $b_0$  on the wave frequency and wavelength in soils.  $b_0$  becomes progressively smaller if the wave frequency becomes lower and wavelength becomes longer. It is also

interesting to see that  $b_0$  linearly increases with  $\lambda_{\text{Soil}}$  in Figure 13(b), indicating the influence of slope angles on AF becomes less pronounced if wavelength becomes longer.

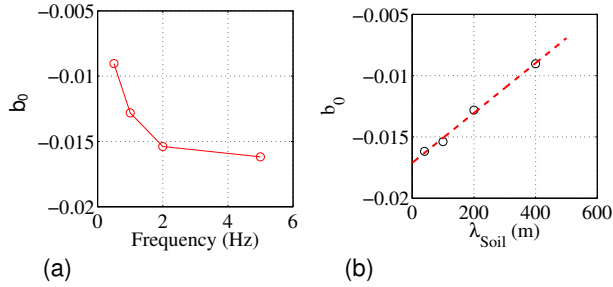


Figure 13: Dependence of  $b_0$  on wave frequency and wavelength in soils

Statistical analyses are performed to evaluate the importance of incorporating the slope angle into the prediction. For this purpose,  $\ln(\text{AF})$  is predicted by only using the linear term of  $C_s$  in Eq. 5, as compared with  $\ln(\text{AF})$  estimated using Eq. 5 with the slope angle term. Figure 14 shows the coefficient of determination  $R^2$  and the standard deviation of the residual term  $\epsilon$  using two models.

It is found that adding the slope angle term can significantly improve the prediction. The slope angle plays an important role when the soil depth is within the range of  $(0.1 \sim 0.2) \lambda_{\text{Soil}}$ . In the meanwhile, the standard deviation of the residuals,  $\sigma = \text{std}(\epsilon)$ , reduces by around 0.05-0.07 in this range. Figure 13 also shows that the standard deviation of the residuals for Eq. 5 generally falls into the range of 0.1-0.15, and increases with increasing soil depths. That means, the majority of the computed data falls within 10-15% around the prediction.

## 5 CONCLUSIONS AND DISCUSSIONS

In this study, we conducted a region-scale 3D numerical simulation to quantify ground-motion amplification considering 3D topography and subsurface soil conditions, using the Hong Kong island as a testbed.

If only a homogenous rock site is considered, the amplification factor can be well correlated with topographic curvature smoothed over a characteristic length, which is half of the wavelength in rock ( $L_s = 1/2\lambda_{\text{Rock}}$ ). The numerical analyses revealed that the topography amplification is frequency dependent, and the maximum values range from 1.6 to 2.0 for different input frequencies.

Considering a layer of surface soil on 3D topography, the ground-motion amplification pattern is significantly influenced by the soil depth. Compared with the homogeneous rock case, the amplification pattern becomes more closely correlated to small-scale topographic features due to the existence of the surface soil. When both topography amplification and soil amplification are considered, the total amplification factor could be greater than 4 compared with the rock outcrop motion when the soil depth is  $0.2\lambda_{\text{soil}}$ .

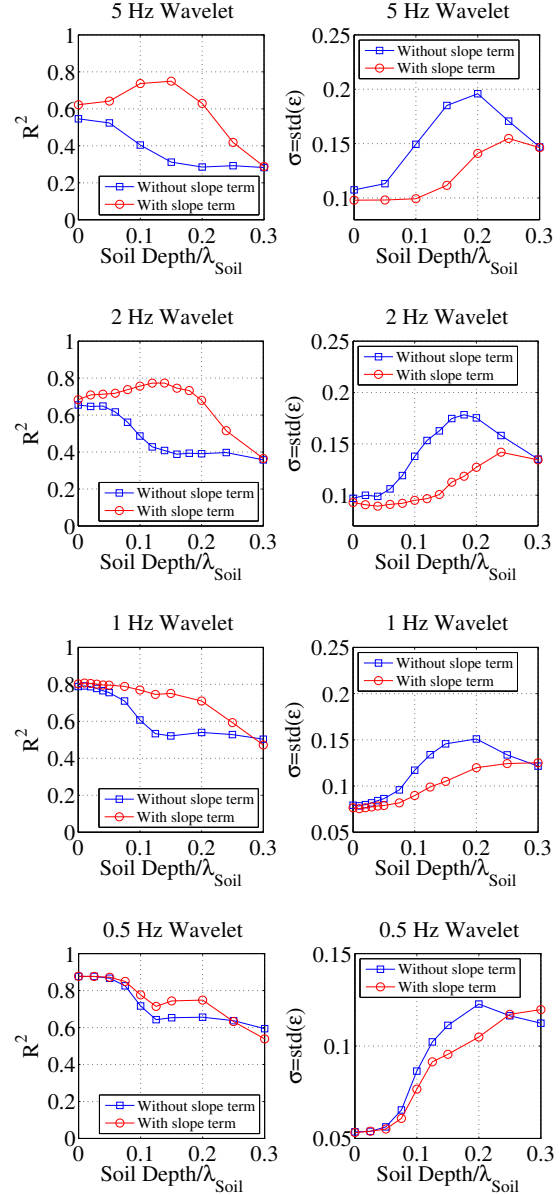


Figure 14.  $R^2$  and standard deviation of residuals obtained using the prediction equation with and without the slope angle term.

Finally, unified prediction equations are proposed to parameterize the ground-motion amplification for different wave frequencies and soil depths using curvatures smoothed over a modified characteristic length and the slope angles. The standard deviation of residuals of the prediction model generally falls between 0.1-0.15, indicating high accuracy of the model. Note that the present study is limited to elastic layered soils without considering material nonlinearity and material damping. Extensive parametric study needs to be performed in the future to quantify the uncertainty of the numerical simulations through varying stratification and properties of soil/rock units.

## ACKNOWLEDGEMENTS

This project is financially supported by General Research Fund No. 16213615 and the Collaborative Research Fund CityU8/CRF/13G provided by the Hong Kong Research Grants Council.

## REFERENCES

- Arup. 2012. *Final report on overall seismic hazard assessment. Pilot seismic microzonation study in north-west New Territories for the study of potential effect of earthquake on natural terrain investigation.* CEDD Agreement No. CE49/2008(GE), Hong Kong.
- Ashford, S.A. Sitar, N. Lysmer, J. and Deng, N. 1997. Topographic effects on the seismic response of steep slopes, *Bulletin of the seismological society of America* 87(3): 701-709.
- Assimaki, D. Gazetas, G. and Kausel, E. 2005. Effects of local soil conditions on the topographic aggravation of seismic motion: parametric investigation and recorded field evidence from the 1999 Athens earthquake, *Bulletin of the Seismological Society of America*, 95(3): 1059-1089
- Burjáněk, J. Edwards, B. and Fäh, D. 2014. Empirical evidence of local seismic effects at sites with pronounced topography: A systematic approach, *Geophysical Journal International*, ggu014.
- CEN. 1998. *Eurocode 8: Design provisions for earthquake resistance of structures. Part 5: Foundations, retaining structures and geotechnical aspects*, CEN, Brussels, Belgium
- Komatitsch, D. and Vilotte, J.P. 1998. The spectral element method: An efficient tool to simulate the seismic response of 2D and 3D geological structures, *Bulletin of the seismological society of America*, 88(2): 368-392.
- Komatitsch, D. Liu, Q. Tromp, J. Süß, P. Stidham, C. and Shaw, J.H. 2004. Simulations of ground motion in the Los Angeles basin based upon the spectral-element method. *Bulletin of the Seismological Society of America*, 94(1): 187-206
- Maufroy, E. Cruz-Atienza, V.M. Cotton, F. and Gaffet, S. 2015. Frequency-Scaled Curvature as a Proxy for Topographic Site-Effect Amplification and Ground-Motion Variability. *Bulletin of the seismological society of America*, 105(1): 354-367.
- Ministry of Construction of P.R. China 2010. *Code for seismic design of buildings*, China Architecture & Building Press, Beijing, China
- Moore, I.D. Grayson, R.B. and Ladson, A.R. 1991. Digital terrain modelling: a review of hydrological, geomorphological, and biological applications. *Hydrological Processes*, 5(1): 3-30.
- Spudich, P. Hellweg, M. and Lee, W.H.K. 1996. Directional topographic site response at Tarzana observed in aftershocks of the 1994 Northridge, California, earthquake: implications for mainshock motions. *Bulletin of the Seismological Society of America*, 86(1B): 193-S208.
- Trifunac, M.D. and Hudson, D.E. 1971. Analysis of the Pacoima dam accelerogram—San Fernando, California, earthquake of 1971. *Bulletin of the Seismological Society of America*, 61(5): 1393-1411.
- Wang, G. Du, C. and Huang, D. 2016. Topographic amplification of ground motions: a case study of Hong Kong, *1st International Symposium on Soil Dynamics and Geotechnical Sustainability*, Hong Kong, 29-33
- Zevenbergen, L.W. and Thorne, C.R. 1987. Quantitative analysis of land surface topography. *Earth surface processes and landforms*, 12(1): 47-56.